High Selectivity of Visible-Light-Driven La-doped TiO$_2$ Photocatalysts for NO Removal

Yu Huang[1], Jun-Ji Cao[1], Fei Kang[2], Sheng-Jie You[2], Chia-Wei Chang[2], Ya-Fen Wang[2*]

[1] *Key Laboratory of Aerosol Chemistry and Physics, Institute of Earth Environment, Chinese Academy of Sciences, Xi'an 710061, China*
[2] *Department of Environmental Engineering, Chung Yuan Christian University, Taoyuan 32023, Taiwan*

ABSTRACT

Semiconductors mediated by rare earth metals (REMs) have attracted attention with regard to the degradation of pollutants. In order to enhance the visible response of TiO$_2$, La-doped TiO$_2$ (La-TO) photocatalysts with visible-light-driven capacity for NO removal were successfully synthesized in this study via a facile sol-gel method followed by calcination. A series of La-TiO$_2$ samples with differing weight ratios were evaluated for their photocatalytic performances. It was found that 3% La integrated with TiO$_2$ (in mass ratio) could enhance the removal efficiency of NO (up to 32%) under solar light, which is more than twice that seen with pure TiO$_2$. The resulting products were characterized by a series of techniques, such as XRD, FTIR, UV-vis DRS, BET and (photo)electrochemical analysis. The results indicated that La-doped TiO$_2$ can harvest visible light due to the relatively narrow band gap (from 2.98 to 2.75 eV). More importantly, La dopant improved electron-hole separation and suppressed charge carrier recombination, due to the synergistic effect. Furthermore, La-doped TiO$_2$ increased the photo-oxidation efficiency of the transformation from NO to NO$_3^-$, owing to inhibition of the production of intermediate NO$_2$ (0.02%). To the best of our knowledge, this study is the first time that La-doped TiO$_2$ has been used to eliminate NO (at the ppb level) in the atmosphere. This study provides a facile and controllable route to fabricate La-TO photocatalyst for NO abatement with high selectivity of NO$_2$ under visible light.

Keywords: La-doped; TiO$_2$; Photocatalysis; NO removal.

INTRODUCTION

NO$_x$, which typically refers to NO and NO$_2$, has been associated with Chinese haze and secondary organic aerosols (SOAs) in recent years (Huang *et al.*, 2014; Shi *et al.*, 2015; Fujitani *et al.*, 2017). The previous literature notes the formation of fine particulate matter (PM, especially PM$_{2.5}$) generated from such chemical precursors, which form *via* photochemical reactions between NO$_x$ and volatile organic compounds (VOCs) (Li *et al.*, 2015a; Wang *et al.*, 2016a; Zhao *et al.*, 2016). It is reported that anthropogenic sources of NO$_x$, which come from stationary power (mainly coal) plants and automobile engines, contribute to the emission and accumulation of NO$_x$ in rapidly urbanizing cities (Ball *et al.*, 1999; Lasek *et al.*, 2013, Liu *et al.*, 2017a). Over the past few decades, DeNO$_x$ catalysis techniques such as selective catalytic reduction (SCR), three-way catalysis (TWC) and wet scrubbing, have been developed to reduce the exhaust

gas in after-treatment systems (Granger and Parvulescu, 2011; Lasek *et al.*, 2013, Liu *et al.*, 2017b). However, these technologies inevitably require the use of noble metals, high temperatures and high costs for the high-concentration NO$_x$ treatment that is part of the process. Photocatalysis, which mainly refers to heterogeneous catalysis, offers an innovative and promising approach to reduce NO$_x$ at the part-per-billion (ppb) level (Wang *et al.*, 2016c; Zhang *et al.*, 2016).

Titania (TiO$_2$) is a well-known semiconductor material that has been employed commercially for a few years (Tong *et al.*, 2012; Kaminski *et al.*, 2015). Titania has been explored for applications in many areas, such as photocatalysis, photovoltaics, water splitting (Chen and Mao, 2007; Thunyasirinon *et al.*, 2015). Owing to such features as abundance, long-term stability against photochemical corrosion and being non-poisonous, huge efforts have been dedicated to utilizing TiO$_2$ in photocatalysis (Devi and Kavitha, 2014; Yu *et al.*, 2016). Nonetheless, it is not feasible to use TiO$_2$ to harvest visible light, because of the limitation of its bandgap (~3.0–3.2 eV). This means that TiO$_2$ can only absorb UV light with a wavelength < 380 nm, and UV light accounts for a very small portion (5%) of solar light. Two key aspects of photocatalysis are the effective harvesting of solar

---

* Corresponding author.
 Tel./Fax: +886-32654912
 E-mail address: yfwang@cycu.edu.tw

energy and suppression of charge carrier recombination. Therefore, one challenge in materials chemistry and physics is to design semiconductor-mediated photocatalysts with a visible-light-harvesting capability and high quantum yield (Wang *et al.*, 2014; Li *et al.*, 2015b).

With these considerations in mind, researchers have examined a number of strategies to broaden the spectral absorption range of TiO_2. Numerous approaches have been proposed, including doping, the use of co-catalysts with foreign ions, the application of surface plasmon resonance (SPR) effects, Schottky junctions and the construction of heterojunctions (containing type-I and type-II heterojunctions, Z–scheme, and p–n heterojunctions), and these have been reported to effectively increase visible-light absorption, promote the separation and transportation of the charge carriers, and enhance photocatalytic stability (Rajh *et al.*, 1999; Dinh *et al.*, 2014; Ilkhechi *et al.*, 2017). Among the various approaches, non-metal/metal doping into titania has drawn significant attention due to its ability to modify the surface-electronic properties that benefit the photocatalytic quantum yield. For non-metal ion dopants, substitution of p block elements (B, C, N, F, S, P and I) either at Ti^{4+} and O^{2-} sites is an appealing option to tailor the bandgap absorption to the visible-light region, with a robust interfacial charge carrier transfer process (Devi and Kavitha, 2013). For instance, N-doping TiO_2(N-TiO_2) generates the visible light response because of the occupied N $2p$ states above the VB edge, while the transition from the occupied π^* character N–O localized state results in a visible light response for N–TiO_2 (Di Valentin *et al.*, 2005). On the other hand, many transition metal ions have been introduced into titania to extend the visible absorption, which is attributed to the charge transfer transition between the d electrons of the dopant and CB (or VB) of TiO_2. Moreover, metal ions modulate the charge carrier equilibrium concentration by serving as electron–hole traps (Bouras *et al.*, 2007; Murakami *et al.*, 2008; Yu *et al.*, 2009).

In recent years, the doping of rare earth metals (REMs) has offered another simplified approach to extend the light absorption range and prevent the recombination of electron-hole pairs (Yurtsever and Ciftcioglu, 2017). Previous studies showed that REMs having incompletely occupied $4f$ and empty $5d$ orbitals often act as promote catalysis. Doping TiO_2 with REMs can enhance the light absorption by tuning the phase structure, surface area and morphology (Yao *et al.*, 2012). It has been shown that REM doping inhibits the phase transformation of TiO_2 from anatase to rutile, while lanthanum (La) doping can improve photocatalytic performance by increasing the surface area, pore volume, adsorption capacity and electron-hole separation effect (Raza *et al.*, 2015; Shin *et al.*, 2017). Overall, earlier studies with respect to La dopant have mostly focused on its application in the photocatalytic degradation of dyes in wastewater (Huixian *et al.*, 2011; Wang *et al.*, 2016b).

Herein, La-doped TiO_2 (La-TO) photocatalysis with visible-light-driven capacity was successfully synthesized via a facile sol-gel method followed by calcination. To the best of our knowledge, this is the first time that La-doped TiO_2 has been applied in eliminating NO (at the ppb level)

in the atmosphere. The experimental results show that this approach has three advantages compared with pure TiO_2: (1) La-doped TiO_2 can harvest visible light due to the relatively narrow band gap, which contributes to enhancing the removal efficiency of NO (up to 32%); (2) La dopant improves electron-hole separation and suppresses charge carrier recombination; (3) La-doped TiO_2 increases the photo-oxidation efficiency of the transformation from NO to NO_3^-, due to inhibiting the production of intermediate NO_2 (0.02%). Furthermore, a series of La-TO samples with differing weight ratios were evaluated with regard to their photocatalytic performances.

METHODS

Preparation of Pristine TiO_2 and La-TiO_2 Samples

All the chemicals used in our experiment were of analytical grade and applied without further purification. The La-TiO_2 photocatalyst was prepared by a sol-gel method followed by calcination. In brief, 1.5 mL acetic acid and 18 mL absolute ethanol were mixed together (denoted as solution A). Two mL titanium(IV) isopropoxide (Ti(OBu)$_4$) was dissolved into 18 mL absolute ethanol with stirring for several minutes (denoted as solution B). Solution A was then added dropwise into solution B with strong stirring for 30 min. A transparent sol was then obtained and the gelation was finished by aging the sol for 2 h at room temperature. Solution C contained 10 mL H_2O and different mass ratios of La(NO$_3$)$_3$ in the required stoichiometry, and this was slowly added dropwise into the above sol. The gel was dried at 100°C for 12 h after adding 1 mL nitric acid (68%). Finally, the powder samples were calcined at 500°C for 4 h and La-doped TiO_2 samples were obtained. For convenience and clarity, the synthesized La-TiO_2 with various mass ratios of La^{3+} dopant were denoted as La$_x$-TO, where x represents the mass ratio of La^{3+} to La-TiO_2. The resulting samples with x values of 0.5, 1, 2, 3 and 5% were thus labeled as La$_{0.5}$-TO, La$_1$-TO,La$_2$-TO, La$_3$-TO and La$_5$-TO, respectively. For comparison, pure TiO_2 was prepared under the identical conditions without the addition of solution C.

Characterization

The crystalline phase of the as-obtained samples was determined by using an X-ray powder diffractometer (XRD; PANanalytical, X'pert, the Netherlands) with a Cu Kα radiation source (λ = 1.5406 Å) at a scan step size of 0.017° in the 2θ range of 10°–80°. The Brunauer–Emmett–Teller (BET) surface area and pore structure of the samples were obtained from the adsorption branch of the isotherms and the Barrett–Joyner–Halenda formula at 77 K by using a Gemini VII 2390 analyzer (Micromeritics Instrument Corp., Norcross, GA, USA). The optical properties of the catalysts at 200–800 nm were obtained using a Varian Cary 100 Scan UV-Visible system (UV-Vis; Agilent Corp., USA) equipped with Labsphere diffuse reflectance device. Ba$_2$SO$_4$ was used as a reflectance standard. Fourier transform infrared (FT-IR) spectra data were recorded on an FTIR absorption spectrometer (Vertex 70, Bruker), with KBr as the diluent. Photoluminescence (PL; F-7000, Hitachi, Japan) was also

obtained to investigate the optical properties of the resulting samples.

Photocatalytic Activity Assessment

The photocatalytic activities of the as-prepared samples were investigated by degrading NO at ppb levels in a continuous flow reactor at ambient temperature under visible light and with solar light irradiation. The reaction chamber was a rectangular stainless-steel vessel (30 cm L × 15 cm W × 10 cm H) covered with a quartz window. Visible light was provided by a 300 W xenon lamp (Perfect Light MICROSOLAR 300, Beijing, China) with a UV cutoff filter ($\lambda > 420$ nm), which passed vertically through the quartz window. The commercial 300 W Xe arc lamp (MICROSOLAR 300 UV, Beijing) for the simulated solar light photocatalytic activity test was placed vertically 20 cm above the reactor. For each photocatalytic activity experiment, one sample dish (diameter = 12 cm) containing the photocatalyst powders was placed at the center of the reactor. The photocatalyst samples were prepared by coating an aqueous suspension of the products onto a glass dish. The weight of the photocatalysts used for each experiment was maintained at 100 mg. The dishes containing the photocatalyst were pretreated at 70°C for several hours until water in the suspension was completely removed. The pretreated dishes were then cooled to room temperature prior to the photocatalysis test.

NO gas at an original concentration of 50 ppm was obtained from a compressed gas cylinder. The original concentration of NO used in the photocatalysis test was diluted to 400 ppb with an air stream supplied by a zero air generator (Model 1001, Sabio Instruments LLC, Georgetown, TX, USA). The desired humidity level of the NO flow was controlled at 70% by passing the zero air streams through a humidification chamber. The gas streams were completely premixed by a gas blender, and the flow rate was controlled at 3 L min^{-1} by using a mass flow controller. After the catalyst achieved adsorption/desorption equilibrium, the xenon lamp was switched on. The NO and NO_2 concentrations were continuously measured with a chemiluminescence NO_x analyzer (Model 42c, Thermo Environmental Instruments Inc., Franklin, MA, USA) during photocatalytic degradation at a sampling rate of 0.6 L min^{-1}. The reaction between NO and air was negligible in the control experiment performed with or without light in the absence of the photocatalyst. The removal ratio of NO at any onetime was noted as ($1 - C/C_0$), where C is the NO concentration of the outlet at any one time, and C_0 is the initial concentration of NO, ppb. The selectivity of NO_2 over different photocatalysts was calculated by the following equation (Zhang *et al.*, 2016):

$$NO_2 \text{ yields } = \frac{C_{NO_2}}{C_0 - C} \times 100\% \tag{1}$$

where C_{NO_2} is the production of NO_2, ppb.

Photoelectrochemical Measurements

The photoelectrochemical properties of the as-prepared samples were measured using an electrochemical workstation (PARSTAT-4000, Advanced Measurements Technology, Inc., USA) with a conventional three-electrode cell, which includes a platinum plate and an Ag/AgCl electrode that act as a counter electrode and a reference electrode, respectively. Afterward, La-TiO_2 (25 mg) was dispersed into 5 mL of 1 wt% Nafion ethanol solution to obtain a homogeneous suspension *via* bath sonication and thus fabricate a working electrode. The films were subsequently modified by a 10 mm × 10 mm fluorine-doped tin oxide conducting glass by using a dip coater (ZR-4200, Qingdao, China). The modified films were then arranged to dry under ambient conditions. A 300 W Xe arc lamp (Perfect Light MICROSOLAR 300, Beijing, China) with a UV cut-off filter ($\lambda > 420$ nm) was employed as a light source. Current–time curves were tested at 0.2 V versus Ag/AgCl in Na_2SO_3(0.1 mol L^{-1}) at ambient temperature.

RESULTS AND DISCUSSION

Characterization of La-TiO₂

XDR analysis In order to determine the crystal phase of the prepared La-TO, the powder X-ray diffraction patterns were used to investigate the La^{3+} doping on the anatase phase of TiO_2 at different calcination temperatures. Before doping with La^{3+}, the effects of calcination temperature on the structure phase of pure TiO_2 were studied by XRD. As shown in Fig. 1(A), the peaks located at 25.3°, 37.8° and 48.1° show the characteristic diffractions of the (101), (004) and (200) anatase-type TiO_2, which can be well-indexed as the phase of anatase (JCPD no.21-1272). This means that pure anatase was synthesized at 500°C, and the degree of crystallinity degree of TiO_2 was relatively poor at 400°C. Moreover, the phase transformation of TiO_2 from anatase to rutile occurred at 600°C. The Scherrer equation was applied to evaluate the crystallite sizes of the samples, using the following formula:

$$D = \frac{k\lambda}{\beta cos\theta} \tag{2}$$

where D is the average crystallize size (nm), λ is the wavelength of Cu Kα X-ray radiation ($\lambda = 0.15406$ nm), k is a coefficient usually taken as 0.94, β is the full width at half maximum (FWHM) intensity of the peak observed at 2θ. From the equation, the wider FWHM is, the smaller the crystallite size. Fig. 1(B) shows that La^{3+} doping not only inhibited the phase transformation of TiO_2 from anatase to rutile at 600°C, but also decreased the crystallite size of La$_3$-TO. According to previous research, this is because the surrounding La^{3+} combined with Ti^{4+} and formed a Ti-O-La bond. Furthermore, the La$_2O_3$ lattice locks the Ti-O species at the interface, with titania domains preventing the nucleation that is necessary for the transformation of anatase to rutile, resulting in a decrease of the crystallite size of TiO_2 (Lin and Jimmy, 1998). Overall, La$_3$-TO obtained at 500°C was chosen as the optimum sample due to the excellent crystallization of anatase and smaller size.
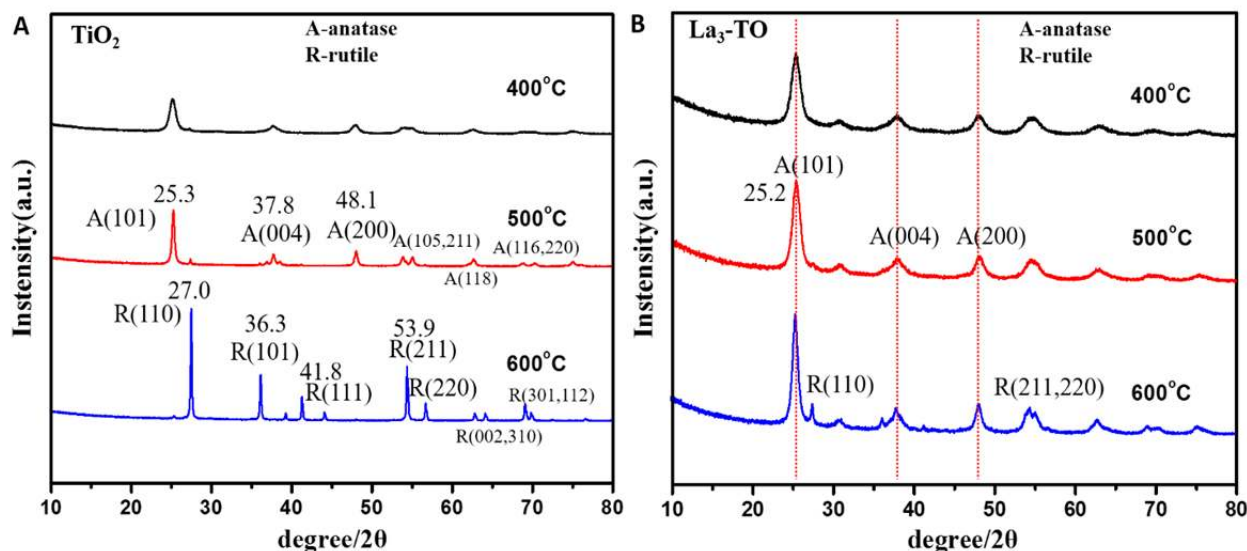
Fig. 1. Powder XRD patterns of as-prepared TiO_2 (A) and La_3-TO (B) at different calcination temperatures (400, 500 and 600°C).

Surface Area and Pore Structure of Samples (BET)

As shown in Fig. 2, the N_2 adsorption-desorption isotherms were measured to analyze the surface area and porosity. The results showed that all isotherms are of a type Langmuir IV isotherm with an H2 hysteresis loop according to the IUPAC classification, which indicates the presence of mesopores (Thommes *et al.*, 2015). Pure TiO_2 and La_3-TO exhibited mesoporosity with average pore sizes approximating 3.45 nm and 5.47 nm, respectively. The BET specific surface areas, pore volume and pore diameters of the samples are given in Table 1. The specific surface area of the La_3-TO calcined at 500°C is 101.90 $cm^3\,g^{-1}$, which is four times larger than that of pure TiO_2 (23.47 $cm^3\,g^{-1}$). The relatively high surface area of La^{3+} doped samples confirms that the frameworks of TiO_2 have better adsorption ability. This may be due to the linkage between the rare earth ions and titanium by the oxygen bridge, which effectively enhances the specific surface area of TiO_2 (Huixian *et al.*, 2011). Overall, the results indicate that La_3-TO has the better photocatalytic activity, which may be due to the existence of a mass of surface active sites.

FTIR and UV-vis Analysis

The FTIR spectra of pure TiO_2 and La_3-TO are shown in Fig. 3(A), in which a series of typical absorption bands of pure TiO_2 and La_3-TO can be observed. The absorption bands at 3414 cm^{-1} and 1635 cm^{-1} indicate the characteristic vibration mode of O-H, demonstrating that much more H_2O adsorbed on the surface of La_3-TO after doping with La^{3+}, which was then capable of producing much more •OH radicals after light irradiation. The absorption band at 530 cm^{-1} is assigned to the characteristic vibration mode of Ti-O-Ti. To investigate the optical absorption properties of photocatalysts, the UV-vis DRS of pureTiO_2 and La_3-TO in the range of 200–800 nm were measured and the results are shown in Fig. 3(B). The spectra of La_3-TO show red shift compared with pure TiO_2. This phenomenon can be attributed to the charge-transfer transition between 4*f* orbital electrons of rare earth ions and the TiO_2 conduction or valence band (Borgarello *et al.*, 1982). Therefore, titania doped with La^{3+} increased the absorption range in the visible-light region. Moreover, the band energies (Eg), which are estimated from the intercept of tangents to the plots of $(\alpha h\nu)^{1/2}$ versus the photo energy, are 2.98 and 2.75 eV for pure TiO_2 and La_3-TO, respectively, as illustrated in Fig. 3(B). It was thus found that La^{3+} dopant narrowed the band gap of TiO_2, which extended the optical response in the visible-light region.

Photocatalytic Activity Assessment

The photocatalytic activities of blank (direct photolysis), pure TiO_2 and La_x-TO with different La-doped mass ratios ($x = 0.5, 1, 2, 3$ and 5%) were evaluated for the degradation of NO under visible light ($\lambda > 420$ nm) and under solar light irradiation. The NO removal rates against irradiation time over different photocatalysts are plotted in Figs. 4(A) and 4(B). It can be seen that the pristine TiO_2 had poorer photocatalytic performance for NO removal under visible light (only 2.8%), as relatively broad bandgap of TiO_2 can only be stimulated by UV. In contrast, the use of La_x-TO with varying amounts of dopant dramatically improved the photocatalytic efficiency. Moreover, the degradation efficiency increased along with the amount of La^{3+} dopant. In particular, La_3-TO exhibited the highest photocatalytic activity (up to 29%) and continued with the degradation even when irradiated for 30 min, with this activity being 10 times higher than that seen with pure TiO_2. With respect to photocatalytic efficiency under solar light irradiation, La_3-TO also showed 38.5% photocatalytic activity. As for pure TiO_2, it became inactivate after being irradiated for 5 min due to the lack of sufficient •OH radicals. This is in accordance with the FTIR results and the higher specific surface areas of the La_3-TO sample. Moreover, toxic intermediate NO_2 was also identified during the photocatalytic processes. As
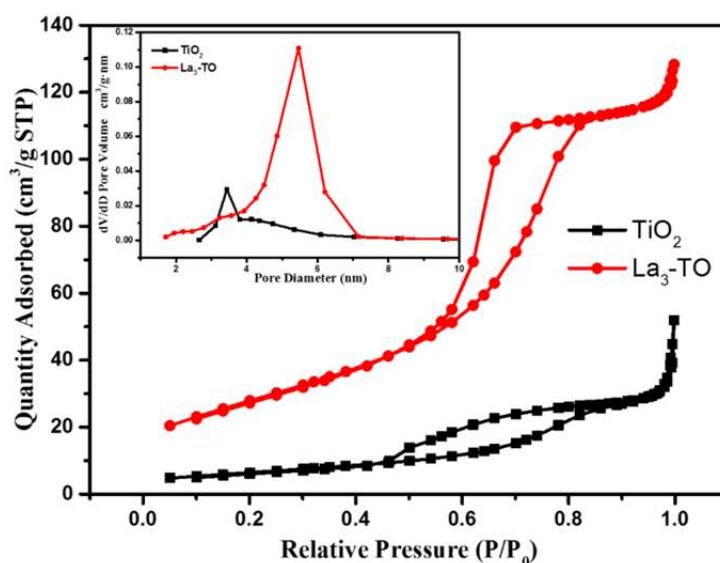
Fig. 2. N_2 sorption isotherms of pure TiO_2 and La_3-TO. Inset: BJH pore size distributions of each sample.

Table 1. Summary of surface area, and pore diameter of pure TiO_2 and La_3-TO.

	TiO_2	La_3-TO
Surface Area ($m^2 g^{-1}$)	23.47	101.90
Pore Volume ($cm^3 g^{-1}$)	0.06	0.19
Pore Diameter (nm)	3.45	5.47

shown in Figs. 4(C) and 4(D), the amount of NO_2 generated showed no significant difference under under visible light ($\lambda > 420$ nm). Nonetheless, La_x-TO produced no toxic NO_2 under solar light irradiation (in Fig. 4(D)), compared with pure TiO_2 (approximately 26%). Therefore, La-doped TiO_2 increased the photo-oxidation efficiency of the transformation from NO to NO_3^-, as it inhibited the production of intermediate NO_2. The doped metal species could trap and subsequently transfer the photoexcited electrons on the TiO_2 surface, accelerating the formation of hydroxyl radicals (•OH). •OH can then further convert intermediate NO_2 into NO_3^-.

In Fig. 5(A), the NO_2 yields of as-prepared samples were calculated based on Eq. (1). The NO_2 yield of pure TiO_2 was up to 6.54% under solar light irradiation, which is much higher than that of La_x-TO. Among the various results, La_3-TO has the lowest minimum production rate of intermediate product (0.02%). This suggests that La_x-TO is better for the removal of NO_x under realistic conditions, due to the impact of La^{3+} doping. It is thus found that La_x-TO photocatalyst has excellent performance for NO abatement, with high selectivity of NO_2 under visible light. Various TiO_2-based nanomaterials have been used for NO removal, and Table 2 summarized the details of some of these earlier efforts, including the methodology, initial concentration of NO, amount of catalyst, irradiation light and by-product (NO_2) yield. As a whole, La_3-TO exhibited favorable capabilities with regard to eliminating NO (at the ppb level) with high selectivity of NO_2 under visible light.

Moreover, reproducibility and stability are important if photocatalysts are to be applied in realistic environments. In order to determine the stability of the photocatalyst, multiple runs for the photocatalytic removal of NO with the La_3-TO samples were tested under solar light irradiation. As shown in Fig. 5(B), the NO removal ratio remained high after undergoing five repeated runs. This indicate that La_3-TO has excellent stability with regard to photocatalytic activity, and can be used repeatedly in a realistic environment.

The Effects of Calcination Temperature on NO Removal

To investigate the effects of catalyst structure on photodegradation efficiency, the La_3-TO samples calcined at different temperatures (400, 500, 600°C) were evaluated for the degradation of NO under visible light ($\lambda > 420$ nm) and under solar light irradiation (in Figs. 6(A) and 6(B)). The results showed that the highest degradation efficiency was achieved with the sample calcined at 500°C, which benefited from the excellent crystallization of anatase and smaller size of La_3-TO (as shown in Fig. 1). The photocatalytic activity of La_3-TO fell when the calcination temperature was raised to 600°C and the rutile structure formed. This shows that the anatase crystal structure has better photocatalytic activity than that the rutile structure. Figs. 6(C) and 6(D) show the corresponding NO_2 generation over La_3-TO samples calcined at different temperatures and monitored simultaneously. The results indicate that La_3-TO calcined at 500°C also released the minimum amount of NO_2 under visible light ($\lambda > 420$ nm). Moreover, the effects of calcination temperature on the generation NO_2 under solar light irradiation showed little significant difference. The temperature at 500°C was thus more appropriate for the calcination of La_3-TO.

***Charge Separation by Photoelectrochemical Analysis***

Generally speaking, the charge separation efficiency is a critical factor to improve the activity of photocatalysts. To validate the effects of the La dopant, the transient photocurrent responses of pure TiO_2 and La_3-TO electrodes in on–off cycles under visible light irradiation were examined.
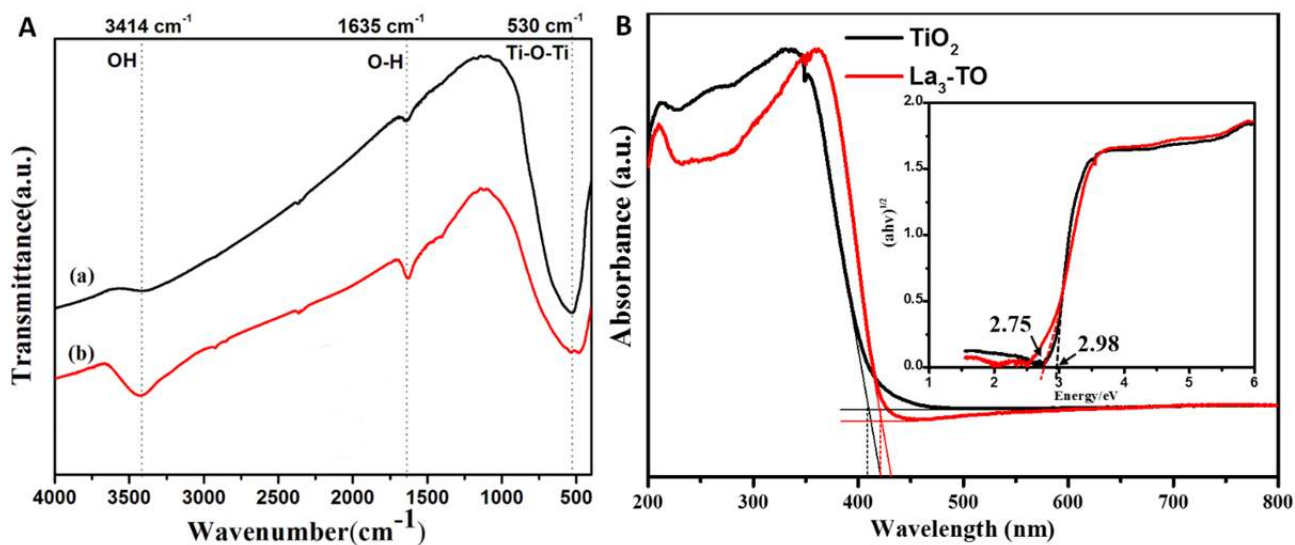
Fig. 3. (A) FTIR and (B) UV-vis DRS spectra of pure TiO_2 (a) and La_3-TO (b). Inset: plots of $(\alpha h\nu)^{1/2}$ versus the photo energy.
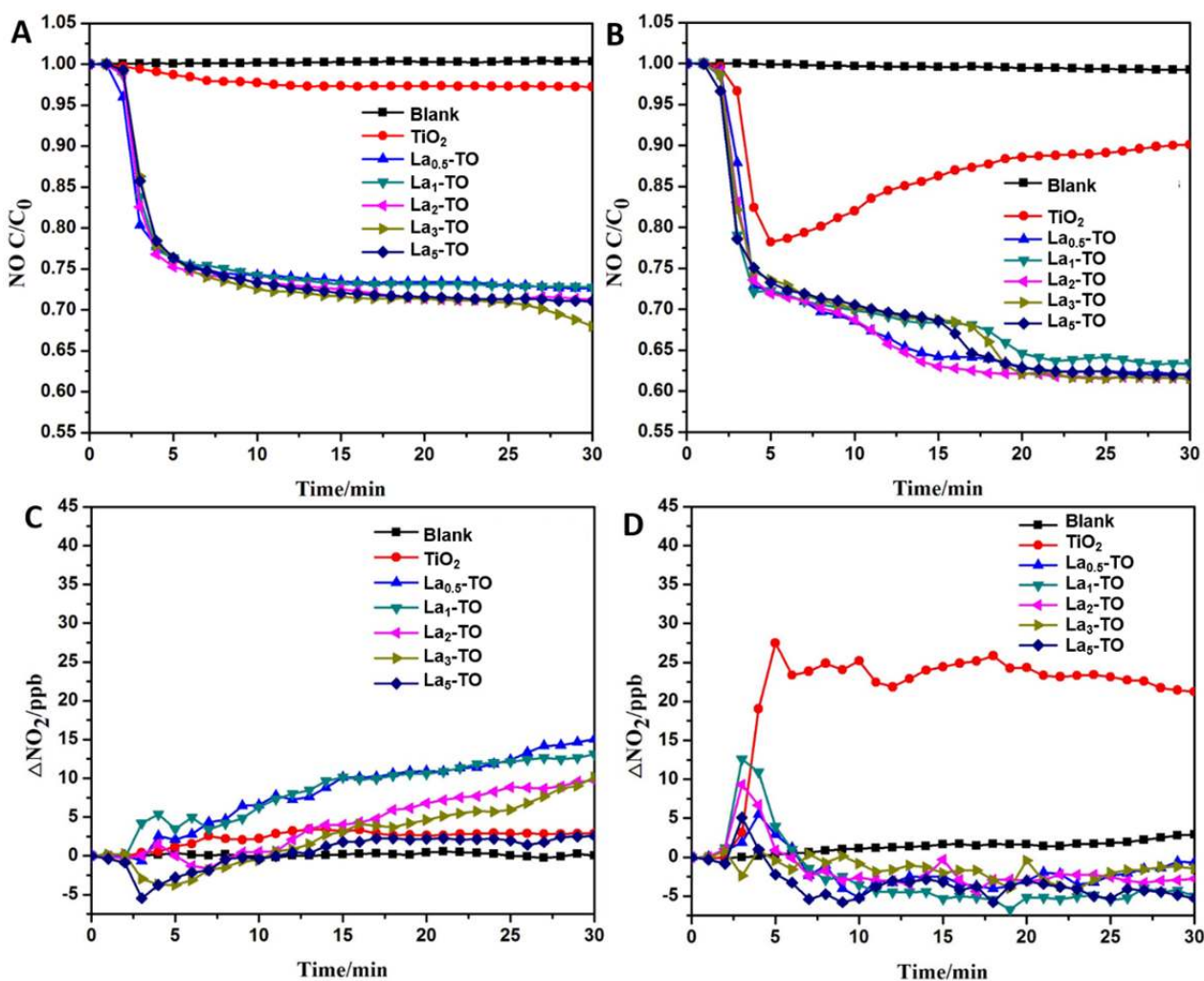
Fig. 4. Photocatalytic activity for NO removal efficiency (C/C_0) against irradiation time over Blank (direct photolysis), pure TiO_2 and La_x-TO with different La-doped mass ratios (A) under visible light ($\lambda > 420$ nm) and (B) under solar light irradiation; the corresponding NO_2 generation against irradiation time (C) under visible light ($\lambda > 420$ nm) and (D) under solar light irradiation.
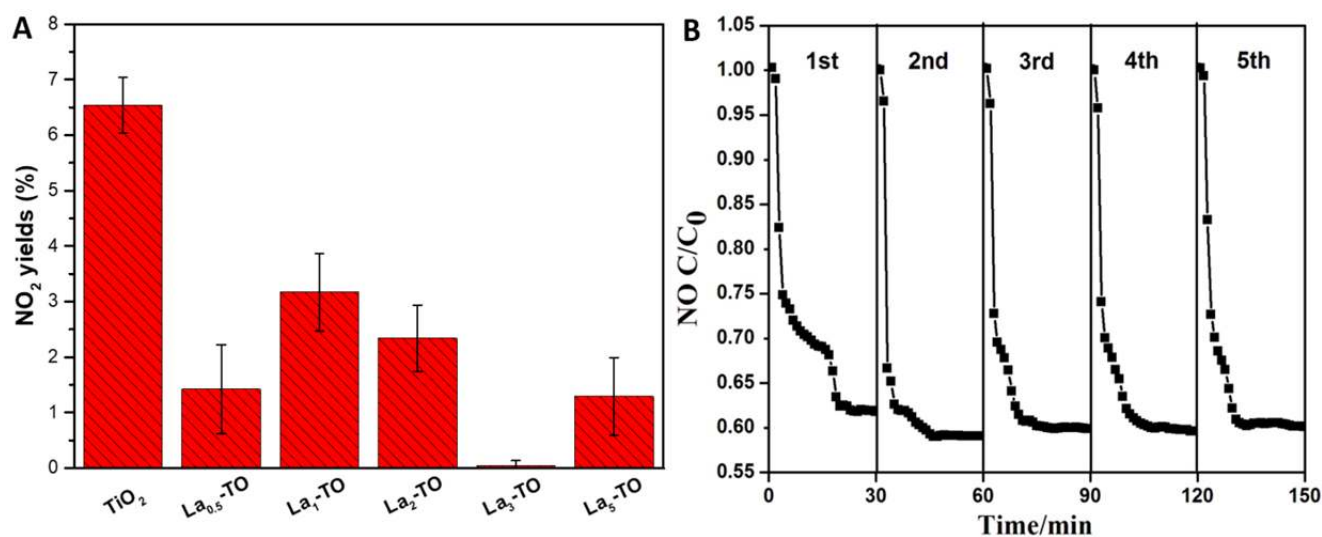
Fig. 5. (A) The corresponding NO_2 yields over pure TiO_2 and La_x-TO under solar light irradiation. (B) Cycling runs for the photocatalytic degradation of NO with La_3-TO under solar light irradiation.

Table 2. Comparison on NO removal efficiency of various TiO_2-based nanomaterials.

Nanomaterials	Method	Experiment condition		NO removal efficiency	NO_2 yield	Reference
		Initial concentration	Amount of catalyst			
Oxygen-deficient TiO_2	Photocatalysis	400 ppb	50 mg	65% (420–700 nm)	15%	(Ma *et al.*, 2014)
P25	Photocatalysis	1000 ppb	16 ± 2 mg	38.0% (solar light)	33.4%	(Fujiwara *et al.*, 2016)
[a]f-TiO_2	Photocatalysis	1000 ppb	16 ± 2 mg	53.0% (solar light)	40.1%	(Fujiwara *et al.*, 2016)
[b]w-Pd/f-TiO_2	Photocatalysis	1000 ppb	16 ± 2 mg	52.0% (solar light)	40.1%	(Fujiwara *et al.*, 2016)
[c]K-MnOx/TiO_2	[d]SCR	720 ppm	2000 mg	80%	—	(Fang *et al.*, 2015)
[e]15%MWCNTs/Cu–TiO_2	Photocatalysis	58.4 ppm	—	46% (365 nm)	—	(Liu *et al.*, 2014)
Pt-doped TiO_2	Photocatalysis	40 ppm	50 mg	35% (visible light)	18%	(Hu *et al.*, 2015)
Ni-doped TiO_2	Photocatalysis	400 ppb	300 mg	45%(solar light)	—	(Huang *et al.*, 2009)
La_3-TO	Photocatalysis	400 ppb	100 mg	32% (solar light)	0.02%	*This work*

[a] f-TiO_2: TiO_2 prepared by flame spray pyrolysis (FSP); [b] w-Pd/f-TiO_2: 1 wt% of Pd was photodeposited on f-TiO_2; [c] K-MnOx/TiO_2: potassium deactivation of MnOx/TiO_2; [d] SCR: selective catalytic reduction; [e] 15%MWCNTs/Cu–TiO_2: 15 mol% Cu doped TiO_2 supported by MWCNTs; —: no relevant report.

As shown in Fig. 7, when the light source was turned on the photocurrent increased rapidly and was very stable, whereas the value decreased immediately after the lamp was turned off, suggesting that the as-prepared electrodes possess fast photoelectric response ability. The highest photocurrent density from La_3-TO at the potential of 0.2 V (about 0.4 uA cm^{-2}) is much higher than that from pure TiO_2 (0.13 uA cm^{-2}). This distinctly enhanced photocurrent density indicates that the doping of La^{3+} can efficiently accelerate the separation of photoexcited electron–hole pairs and inhibit the recombination efficiency of photogenerated carriers.

Possible Photocatalytic Mechanism

Based on the analysis presented above, we then considered the possible photocatalytic mechanism for NO removal over La-doped TiO_2. The reaction processes of the degradation of NO over La-doped TiO_2 are thus explained in the following equations (Reactions 1–7). Once La-doped TiO_2 was irradiated by visible light, photoexcited electrons

and holes were generated (R1). The resulting electrons could transfer onto the surface of La^{3+}, which promotes the separation of electrons and holes. The electrons captured by La^{3+} then reacted with the surrounding oxygen to form •O_2^- radicals (R2). The generated •O_2^- radicals and holes (h$^+$) could directly oxidize NO into the final product NO_3^- (R3 and R4). Moreover, H_2O molecules on the surface of TiO_2 could be oxidized into •OH radicals (R5). Because there are much more •OH radicals, NO could be transferred into NO_3^- by these via two-step oxidation (R6 and R7), which prevents the production of intermediate NO_2. The whole reaction mechanism for NO removal is shown in Scheme 1. Overall, La^{3+} dopant could increase the amount of oxygen vacancies and/or surface defects in the TiO_2 photocatalysts that might capture photoelectrons and inhibit the recombination of photo-generated electrons-holes pairs, which results in greater quantum efficiency (Wang *et al.*, 2011). In summary, La^{3+} dopant showed a synergistic effect for NO removal under visible light.
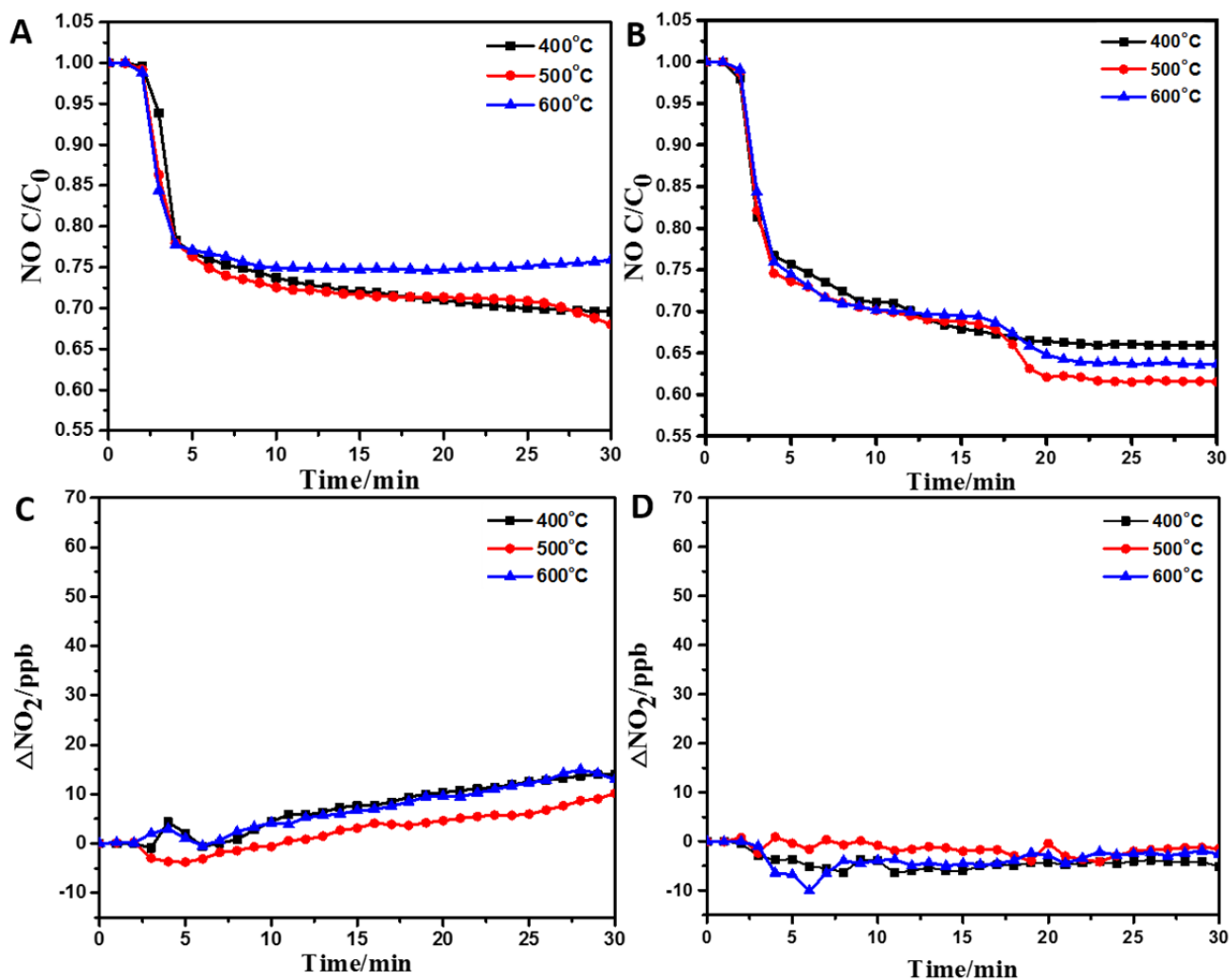
Fig. 6. Photocatalytic activity for NO removal efficiency (C/C_0) against irradiation time over La_3-TO samples calcined at different temperatures (400, 500, 600°C) under visible light ($\lambda > 420$ nm) (A) and under solar light irradiation (B); the corresponding NO_2 generation against irradiation time (C) under visible light ($\lambda > 420$ nm) and (D) under solar light irradiation.
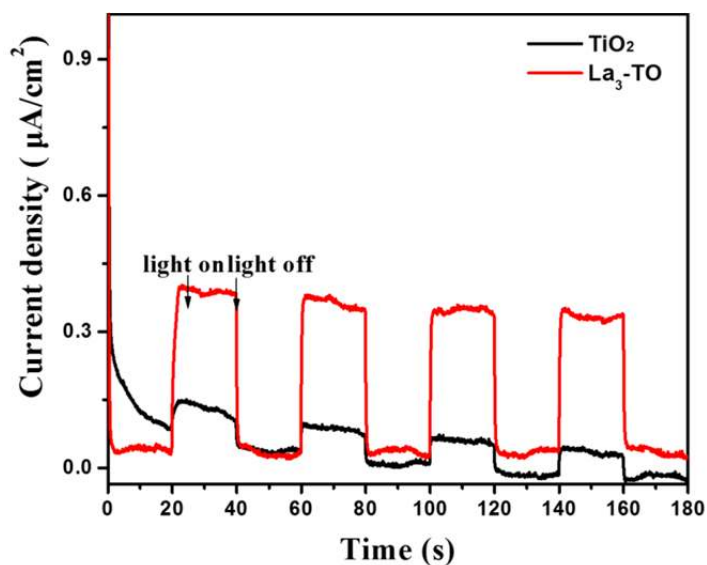
Fig. 7. Photocurrent-time curves of the as-prepared samples.
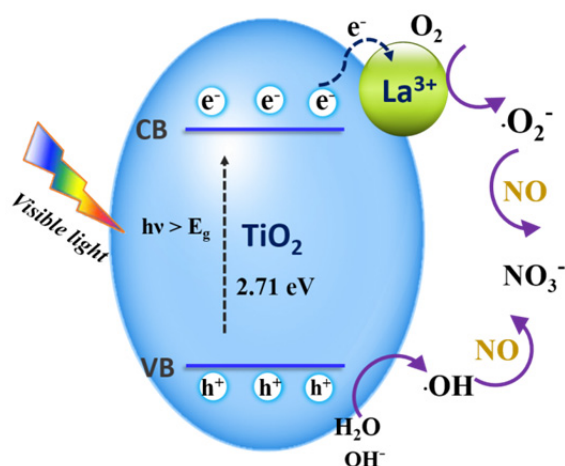
Scheme 1. Mechanism of the synergistic effects of La^{3+} for NO removal under visible light.

$$La\text{-}TiO_2 + hv \rightarrow e^- + h^+ \quad (R1)$$

$$e^- + O_2 \rightarrow \bullet O_2^- \quad (R2)$$

$$h^+ + NO + 2H_2O \rightarrow NO_3^- + 4H^+ \quad (R3)$$

$$\bullet O_2^- + NO \rightarrow NO_3^- \quad (R4)$$

$$h^+ + H_2O \rightarrow \bullet OH \quad (R5)$$

$$2\bullet OH + NO \rightarrow NO_2 + H_2O \quad (R6)$$

$$NO_2 + \bullet OH \rightarrow NO_3^- + H^+ \quad (R7)$$

CONCLUSIONS

In conclusion, La-doped TiO$_2$ (La-TO) photocatalysts were synthesized successfully in this work via a facile sol-gel method followed by calcination. Compared with pure TiO$_2$, La-doped TiO$_2$ dramatically improved the visible light photocatalytic activity with regard to eliminating NO (at ppb level) in the atmosphere, and this is attributed to the fact that La-doped TiO$_2$ can harvest visible light because of the relatively narrow band gap. In addition, La-doped TiO$_2$ can promote electron-hole separation, as La^{3+} can have synergistic effects and capture photoinduced electrons. Notably, La-doped TiO$_2$ increased the photo-oxidation efficiency of the transformation from NO to NO$_3^-$, due to inhibiting the production of intermediate NO$_2$. In short, this study provides a facile and effective approach to prepare La-TiO$_2$ photocatalyst for NO abatement with high selectivity of NO$_2$ under visible light.

ACKNOWLEDGMENTS

DISCLAIMER

The authors declare no competing financial interests.

REFERENCES

Ball, J.C., Hurley, M.D., Straccia, A.M. and Gierczak, C.A. (1999). Thermal release of nitric oxide from ambient air and diesel particles. *Environ. Sci. Technol.* 33: 1175–1178.

Borgarello, E., Kiwi, J., Graetzel, M., Pelizzetti, E. and Visca, M. (1982). Visible light induced water cleavage in colloidal solutions of chromium-doped titanium dioxide particles. *J. Am. Chem. Soc.* 104: 2996–3002.

Bouras, P., Stathatos, E. and Lianos, P. (2007). Pure versus metal-ion-doped nanocrystalline titania for photocatalysis. *Appl. Catal. B* 73: 51–59.

Chen, X. and Mao, S.S. (2007). Titanium dioxide nanomaterials: Synthesis, properties, modifications, and applications. *Chem. Rev.* 107: 2891–2959.

Devi, L.G. and Kavitha, R. (2013). A review on non metal ion doped titania for the photocatalytic degradation of organic pollutants under UV/solar light: Role of photogenerated charge carrier dynamics in enhancing the activity. *Appl. Catal. B* 140: 559–587.

Devi, L.G. and Kavitha, R. (2014) Review on modified N–TiO$_2$ for green energy applications under UV/visible light: Selected results and reaction mechanisms. *Rsc Adv.* 4: 28265–28299.

Di Valentin, C., Pacchioni, G., Selloni, A., Livraghi, S. and Giamello, E. (2005). Characterization of paramagnetic species in N-doped TiO$_2$ powders by EPR spectroscopy and Dft calculations. *J. Phys. Chem. B* 109: 11414–11419.

Dinh, C.T., Yen, H., Kleitz, F. and Do, T.O. (2014). Three-dimensional ordered assembly of thin-shell Au/TiO$_2$ hollow nanospheres for enhanced visible-light-driven photocatalysis. *Angew. Chem. Int. Edit.* 53: 6618–6623.

Fang, D., Xie, J.L., Hu, H., Zhang, Z., He, F., Zheng, Y. and Zhang, Q. (2015). Effects of precursors and preparation methods on the potassium deactivation of MnO$_x$/TiO$_2$ catalysts for NO removal. *Fuel Process. Technol.* 134: 465–472.

Fujitani, Y., Furuyama, A., Tanabe, K. and Hirano, S. (2017). Comparison of oxidative abilities of PM$_{2.5}$ collected at traffic and residential sites in Japan. Contribution of transition metals and primary and secondary aerosols. *Aerosol Air Qual. Res.* 17: 574–587.

Fujiwara, K., Müller, U. and Pratsinis, S.E. (2016). Pd subnano-clusters on TiO$_2$ for solar-light removal of NO. *ACS Catal.* 6: 1887–1893.

Granger, P. and Parvulescu, V.I. (2011). Catalytic NO$_x$ abatement systems for mobile sources: From three-way to lean burn after-treatment technologies. *Chem. Rev.* 111: 3155–3207.

Hu, Y., Song, X., Jiang, S. and Wei, C. (2015). Enhanced photocatalytic activity of Pt-doped TiO$_2$ for nox oxidation both under UV and visible light irradiation: A synergistic effect of lattice Pt^{4+} and surface PtO. *Chem.*

Eng. J. 274: 102–112.

Huang, R.J., Zhang, Y., Bozzetti, C., Ho, K.F., Cao, J.J., Han, Y., Daellenbach, K.R., Slowik, J.G., Platt, S.M. and Canonaco, F. (2014). High secondary aerosol contribution to particulate pollution during haze events in China. *Nature* 514: 218.

Huang, Y., Ho, W., Ai, Z., Song, X., Zhang, L. and Lee, S. (2009). Aerosol-assisted flow synthesis of B-doped, Ni-doped and B–Ni-codoped TiO_2 solid and hollow microspheres for photocatalytic removal of NO. *Appl. Catal. B* 89: 398–405.

Huixian, S.H.I., Zhang, T. and Hongliang, W. (2011). Preparation and photocatalytic activity of La^{3+} and Eu^{3+} co-doped TiO_2 nanoparticles: Photo-assisted degradation of methylene blue. *J.Rare Earth.* 29: 746–752.

Ilkhechi, N.N., Ghobadi, N. and Akbarpour, M.R. (2017). Enhanced optical and photo catalytic properties of V and La co doped TiO_2 nanoparticles. *J. Mater. Sci. - Mater. Electron.* 28: 6426–6434.

Kaminski, H., Beyer, M., Fissan, H., Asbach, C. and Kuhlbusch, T.A.J. (2015). Measurements of nanoscale TiO_2 and Al_2O_3 in industrial workplace environments – Methodology and results. *Aerosol Air Qual. Res.* 15: 129–141.

Lasek, J., Yu, Y.H. and Wu, J.C.S. (2013). Removal of NO_x by photocatalytic processes. *J. Photochem. Photobiol. C* 14: 29–52.

Li, H., Zhou, Y., Tu, W., Ye, J. and Zou, Z. (2015b). State-of-the-art progress in diverse heterostructured photocatalysts toward promoting photocatalytic performance. *Adv. Funct. Mater.* 25: 998–1013.

Li, Y., Zhao, H. and Wu, Y. (2015a). Characteristics of particulate matter during haze and fog (pollution) episodes over northeast China, autumn 2013. *Aerosol Air Qual. Res.* 15: 853–864.

Lin, J. and Jimmy, C.Y. (1998). An investigation on photocatalytic activities of mixed TiO_2-rare earth oxides for the oxidation of acetone in air. *J. Photochem. Photobiol. A* 116: 63–67.

Liu, H., Yu, X. and Yang, H. (2014). The integrated photocatalytic removal of SO_2 and NO using Cu doped titanium dioxide supported by multi-walled carbon nanotubes. *Chem. Eng. J.* 243: 465–472.

Liu, Y., Martinet, S., Louis, C., Pasquier, A., Tassel, P. and Perret, P. (2017a). Emission characterization of in-use diesel and gasoline Euro 4 to Euro 6 passenger cars tested on chassis dynamometer bench and emission model assessment. *Aerosol Air Qual. Res.* 17: 2289–2299.

Liu, H., Zhang, Z., Li, Q., Chen, T., Zhang, C., Chen, D., Zhu, C. and Jiang, Y. (2017b). Novel method for preparing controllable nanoporous α-Fe_2O_3 and its reactivity to SCR De-NO_x. *Aerosol Air Qual. Res.* 17: 1898–1908.

Ma, J., Wu, H., Liu, Y. and He, H. (2014). Photocatalytic removal of NO_x over visible light responsive oxygen-deficient TiO_2. *J. Phys. Chem. C* 118: 7434–7441.

Murakami, N., Chiyoya, T., Tsubota, T. and Ohno, T. (2008). Switching redox site of photocatalytic reaction on titanium(iv) oxide particles modified with transition-metal ion controlled by irradiation wavelength. *Appl.*

Catal. A 348: 148–152.

Rajh, T., Nedeljkovic, J.M., Chen, L.X., Poluektov, O. and Thurnauer, M.C. (1999). Improving optical and charge separation properties of nanocrystalline TiO_2 by surface modification with vitamin C. *J. Phys. Chem. B* 103: 3515–3519.

Raza, W., Haque, M.M., Muneer, M., Fleisch, M., Hakki, A. and Bahnemann, D. (2015). Photocatalytic degradation of different chromophoric dyes in aqueous phase using La and Mo doped TiO_2 hybrid carbon spheres. *J. Alloys Compd.* 632: 837–844.

Shi, K., Liu, C. and Huang, Y. (2015). Multifractal processes and self-organized criticality of $PM_{2.5}$ during a typical haze period in Chengdu, China. *Aerosol Air Qual. Res.* 15: 926–934.

Shin, S.S., Yeom, E.J., Yang, W.S., Hur, S., Kim, M.G., Im, J., Seo, J., Noh, J.H. and Seok, S.I. (2017). Colloidally prepared La-doped $BaSnO_3$ electrodes for efficient, photostable perovskite solar cells. *Science* 356: 167–171.

Thommes, M., Kaneko, K., Neimark, A.V., Olivier, J.P., Rodriguez-Reinoso, F., Rouquerol, J. and Sing, K.S.W. (2015). Physisorption of gases, with special reference to the evaluation of surface area and pore size distribution (IUPAC Technical Report). *Pure Appl. Chem.* 87: 1051–1069.

Thunyasirinon, C., Sribenjalux, P., Supothina, S. and Chuaybamroong, P. (2015). Enhancement of air filter with TiO_2 photocatalysis for mycobacterium tuberculosis removal. *Aerosol Air Qual. Res.* 15: 600–610.

Tong, H., Ouyang, S., Bi, Y., Umezawa, N., Oshikiri, M. and Ye, J. (2012). Nano-photocatalytic materials: Possibilities and challenges. *Adv. Mater.* 24: 229–251.

Wang, G., Zhang, R., Gomez, M.E., Yang, L., Zamora, M.L., Hu, M., Lin, Y., Peng, J., Guo, S. and Meng, J. (2016a). Persistent sulfate formation from London Fog to Chinese haze. *Proc. Natl. Acad. Sci. U.S.A.* 113: 13630–13635.

Wang, H.L., Zhang, L.S., Chen, Z.G., Hu, J.Q., Li, S.J., Wang, Z.H., Liu, J.S. and Wang, X.C. (2014). Semiconductor heterojunction photocatalysts: Design, construction, and photocatalytic performances. *Chem. Soc. Rev.* 43: 5234–5244.

Wang, Q., Xu, S. and Shen, F. (2011). Preparation and characterization of TiO_2 photocatalysts co-doped with iron (iii) and lanthanum for the degradation of organic pollutants. *Appl. Surf. Sci.* 257: 7671–7677.

Wang, Q.H., Gao, X.C., Zhang, R.F., Shen, B.B., Tan, Z.B., Li, Z. and Yu, S.Y. (2016b). Decorated TiO_2 nanoparticles with La and Ag elements to improve photocatalytic activity under visible light for the degradation of Mo. *J. Nanosci. Nanotechnol.* 16: 3587–3591.

Wang, Z., Huang, Y., Ho, W., Cao, J., Shen, Z. and Lee, S.C. (2016c). Fabrication of $Bi_2O_2CO_3$/g-C_3N_4 heterojunctions for efficiently photocatalytic NO in air removal: *In-situ* self-sacrificial synthesis, characterizations and mechanistic study. *Appl. Catal. B* 199: 123–133.

Yao, S., Jia, X., Jiao, L., Zhu, C. and Shi, Z. (2012). La-doped TiO_2 hollow fibers and their photocatalytic activity under UV and visible light. *Indian J. Chem.* 51A: 1049–1056.

Yu, J., Xiang, Q. and Zhou, M. (2009). Preparation, characterization and visible-light-driven photocatalytic activity of Fe-doped titania nanorods and first-principles study for electronic structures. *Appl. Catal. B* 90: 595–602.

Yu, M.F., Lin, X.Q., Li, X.D., Chen, T. and Yan, J.H. (2016). Catalytic decomposition of PCDD/Fs over nano-TiO$_2$ based V$_2$O$_5$/CeO$_2$ catalyst at low temperature. *Aerosol Air Qual. Res.* 16: 2011–2022.

Yurtsever, H.A. and Ciftcioglu, M. (2017). The effect of rare earth element doping on the microstructural evolution of sol-gel titania powders. *J. Alloys Compd.* 695: 1336–1353.

Zhang, Q., Huang, Y., Xu, L., Cao, J.J., Ho, W. and Lee, S.C. (2016). Visible-light-active plasmonic Ag–SrTiO$_3$ nanocomposites for the degradation of NO in air with high selectivity. *ACS Appl. Mater. Interfaces* 8: 4165–4174.

Zhao, M., Xiu, G., Qiao, T., Li, Y. and Yu, J. (2016). Characteristics of haze pollution episodes and analysis of a typical winter haze process in Shanghai. *Aerosol Air Qual. Res.* 16: 1625–1637.